Radiation Measurements 172 (2024) 107068

Contents lists available at ScienceDirect

Radiation Measurements

journal homepage: www.elsevier.com/locate/radmeas

Improvement and verification of new measurement methods for radon and thoron progeny activity concentration based on alpha spectrometry analysis

Kang Peng [a,b], Hao Wang [a,b], Jinmin Yang [b], Lei Zhang [b,*], Qiuju Guo [a]

[a] State Key Laboratory of Nuclear Physics and Technology, School of Physics, Peking University, Beijing, 100871, China
[b] State Key Laboratory of NBC Protection for Civilian, Beijing, 102205, China

ARTICLE INFO

Keywords:
Radon and thoron progeny
Alpha spectrometry method
Activity concentration
Comparison experiment
Methodological sensitivity

ABSTRACT

For accurate dose evaluation of radon and thoron exposure, it is important to find a more effective method to measure radon and thoron progeny activity concentration in field measurements. For the purpose of improving measurement sensitivity, two new alpha spectrometry methods, the Wicke-Tn and PKU-Tn methods, for radon as well as thoron progeny were proposed and a series of verification experiments carried out in different environments. Results showed that the two new methods both gave accurate radon and thoron progeny activity concentration individually, and the methodological sensitivity and uncertainty were greatly improved. In an experimental mixed radon–thoron environment, the methodological sensitivity of the PKU-Tn and Wicke-Tn methods were nearly 9.0 and 3.6 times higher than that of the Kerr-Tn method, respectively. Among the three methods, the PKU-Tn method had the highest methodological sensitivity and lowest uncertainty, indicating its prospects for use in field measurement.

1. Introduction

Radon and thoron are significant sources of human exposure to natural radiation. They contribute approximately half of the total exposure dose from all natural sources of ionizing radiation (UNSCEAR, 2008). Radon progeny are the greatest contributors to human exposure doses, and it has become increasingly clear that the exposure caused by thoron progeny cannot be ignored in some specific environments. Since thoron is usually present together with radon, both radon and thoron progeny can be detected in residential homes as well as workplaces at various concentrations (UNSCEAR, 2019). Accurate and rapid field measurement for radon and thoron progeny concentration is of great significance for both radon exposure dose evaluation and progeny behavior research.

Compared to methods that only measure radon progeny concentration, this paper concentrates on those methods that measure both radon and thoron progeny. Therefore, this paper only reviews common methods for radon/thoron progeny measurement. There are a number of methods for measuring radon and thoron progeny concentration simultaneously, including total α-counting method (Thomas, 1972; Khan et al., 1982; Zhang and Luo, 1983; Bigu and Grenier, 1984; Thiessen, 1994; Stajic and Nikezic, 2015), α spectrometry method (Kerr, 1975; Coté and Townsend, 1981), α-β spectrometry method (Katona et al., 2007), integrated measurement method (Pressyanov et al., 1993) and liquid scintillation method (Chalupnik et al., 2017). Compared with the total α-counting method which requires five counting intervals and the α-β spectrometry method which is easily affected by the β-region background, the α spectroscopy method can directly distinguish the α particles of different energies emitted by ^{218}Po (6.0 MeV), ^{214}Po (7.69 MeV), ^{212}Po (8.78 MeV) and ^{212}Bi (6.1 MeV), and is the currently the most favored method used, especially for portable instruments.

In 1978, Kerr proposed an α spectrometry method to obtain the activity concentration of short-lived radon and thoron progeny by an inverse matrix using five α counts in the region of interest (ROI) of three counting intervals with a sampling time of 10 min and three counting intervals, which began after the termination of sample collection, of 2–12, 15–30 and 200–220 min (Kerr, 1975). In 1981, Cote introduced an α spectrometry method, in which the overall cycle is limited to 70 min, sampling time is set as 0–10 min and counting intervals are 11–25 and 45–70 min. Because the 8.78 MeV α-particle counts in this cycle are quite small, relative deviation of thoron progeny concentrations are consequently too high for use in field measurement (Coté and

* Corresponding author.
E-mail address: swofely@pku.edu.cn (L. Zhang).

https://doi.org/10.1016/j.radmeas.2024.107068
Received 26 October 2023; Received in revised form 28 January 2024; Accepted 30 January 2024
Available online 1 February 2024

Townsend, 1981).

There are two problems limiting the development of thoron progeny measurement in practice: the measurement period usually needs to be quite long due to the long half-life of ^{212}Pb (10.6 h) and the low methodological sensitivity due to separately sampling and detecting. These can mean that a higher sampling flowrate is needed, which is not suitable for field measurements.

For the purpose of measuring the activity concentration of individual radon/thoron progeny in a field environment, it is quite important to improve the methodological sensitivity. In this paper, two new α spectrometry methods for radon and thoron progeny were proposed and a series of verification experiments were carried out in pure and mixed radon/thoron environments, and then the methodological sensitivity and measurement uncertainty are discussed in detail.

2. Materials and methods

2.1. Basic theory

For radon and thoron progeny measurement method based on α spectrometry analysis, two process are usually carried out separately or simultaneously. During the sampling process, the gas in the space is pumped through the filter, and radon and thoron progeny are then collected onto the filter. During the counting process, α-particles emitted from the filter are detected and recorded with different energies. Three assumptions are as follow (Bigu and Grenier, 1984): (1) concentrations of ^{218}Po, ^{214}Pb, ^{214}Bi, ^{212}Pb and ^{212}Bi in the environment remain constant during the sampling process; (2) flowrate remains constant during the sampling process due to a new filter and use of a negative feedback sampling technique; and (3) the filter has the same collection efficiency for different radon/thoron progeny and the detection efficiencies are the same for different α-particles. There are no assumptions about the ratio of radon/thoron progeny, so these methods could be used both indoor and outdoor as well as other environments, as long as the three assumptions above are satisfied.

Due to the quite short half-life of ^{216}Po, α-particles of 6.8 MeV are usually invisible in the α spectrum. Then the activity concentration of individual radon and thoron progeny (^{218}Po, ^{214}Pb, ^{214}Bi, ^{212}Pb and ^{212}Bi) can be calculated using the recurrence formulas discussed by Jenkins (2002) and those α counts in different ROIs. Counts in different ROIs (N_i) can be expressed by the initial activity concentrations of radon and thoron progeny C_i using coefficient matrix $\widehat{K}$ as Eq. (1) (the $\widehat{K}$ matrix elements' expressions are given in the appendix). Through measuring the counts of α-particles in different ROIs (N_i), the activity concentrations of radon and thoron progeny C_i are given by Eq. (2), where matrix $\widehat{M}$ is the inverse matrix of $\widehat{K}$.

$$\begin{pmatrix} N_1 \\ N_2 \\ N_3 \\ N_4 \\ N_5 \end{pmatrix} = \varepsilon_\alpha \bullet F \bullet \varepsilon_F \begin{pmatrix} K_{11} & K_{12} & K_{13} & K_{14} & K_{15} \\ K_{21} & K_{22} & K_{23} & K_{24} & K_{25} \\ K_{31} & K_{32} & K_{33} & K_{34} & K_{35} \\ K_{41} & K_{42} & K_{43} & K_{44} & K_{45} \\ K_{51} & K_{52} & K_{53} & K_{54} & K_{55} \end{pmatrix} \bullet \begin{pmatrix} C_1 \\ C_2 \\ C_3 \\ C_4 \\ C_5 \end{pmatrix} \tag{1}$$

$$\begin{pmatrix} C_1 \\ C_2 \\ C_3 \\ C_4 \\ C_5 \end{pmatrix} = {\varepsilon_\alpha}^{-1} \bullet F^{-1} \bullet {\varepsilon_F}^{-1} \begin{pmatrix} M_{11} & M_{12} & M_{13} & M_{14} & M_{15} \\ M_{21} & M_{22} & M_{23} & M_{24} & M_{25} \\ M_{31} & M_{32} & M_{33} & M_{34} & M_{35} \\ M_{41} & M_{42} & M_{43} & M_{44} & M_{45} \\ M_{51} & M_{52} & M_{53} & M_{54} & M_{55} \end{pmatrix} \bullet \begin{pmatrix} N_1 \\ N_2 \\ N_3 \\ N_4 \\ N_5 \end{pmatrix} \tag{2}$$

where, C_1, C_2, C_3, C_4 and C_5 are the activity concentrations of ^{218}Po, ^{214}Pb, ^{214}Bi, ^{212}Pb and ^{212}Bi (Bq/m^3), respectively; ε_α is the α detection efficiency (dimensionless); F is the sampling flowrate (L/min); and ε_f is the collection efficiency of the filter (dimensionless).

The α spectra obtained during three counting intervals have similar ROIs, denoted ROI-I (6.0 MeV, including α particles from ^{218}Po and a portion of α particles from ^{212}Bi), ROI-II (7.69 MeV) and ROI-III (8.78 MeV).[1] For measuring five individual radon and thoron progeny, five α counts in different ROIs from three counting intervals are needed. Usually N_1 is the net counts in the ROI-I in the first counting interval, N_2 is net counts in ROI-II in the first counting interval, N_3 is net counts in ROI-II in the second counting interval, N_4 is net counts in ROI-III in the second counting interval and N_5 is net counts in ROI-III in the third counting interval (Fig. 1). Of course, there can be slight differences between different measurement methods. The difference mainly lies in measurement cycle, sampling time and counting interval arrangement, which lead to a different $\widehat{M}$ and a different methodology sensitivity as well as stability.

The uncertainties of activity concentration σ_{C_i} are shown as Eq. (3). It is composed of the uncertainty of measurement counts ($\sigma_{N_i} = \sqrt{N_i}$), detection efficiency ($\sigma_{\varepsilon_\alpha}$), collection efficiency (σ_{ε_F}) and flow rate (σ_F), while the uncertainty of sampling as well as counting time are usually ignored.

$$\frac{\sigma_{C_i}}{C_i} = \sqrt{\frac{{M_{i1}}^2 \bullet N_1 + {M_{i2}}^2 \bullet N_2 + {M_{i3}}^2 \bullet N_3 + {M_{i4}}^2 \bullet N_4 + {M_{i5}}^2 \bullet N_5}{\left(M_{i1} \bullet N_1 + M_{i2} \bullet N_2 + M_{i3} \bullet N_3 + M_{i4} \bullet N_4 + M_{i5} \bullet N_5\right)^2} + \left(\frac{\sigma_{\varepsilon_\alpha}}{\varepsilon_\alpha}\right)^2 + \left(\frac{\sigma_{\varepsilon_F}}{\varepsilon_F}\right)^2 + \left(\frac{\sigma_F}{F}\right)^2} \tag{3}$$

2.2. New measurement methods

For the purpose of effectively increasing radon/thoron progeny measurement sensitivity and following the former idea, two new measurement methods were proposed with different sampling and counting times. Information on the sampling and measurement process of the Kerr-Tn method, taken as the reference method, and the two new proposed methods are shown in Fig. 1. The first method is the Wicke-Tn method, which is a further improvement from the optimized Wicke method by adding an extra counting interval to realize thoron progeny measurement simultaneously (Wang et al., 2021). The sampling time of the optimized Wicke method was synchronized with the first counting interval of 0–30 min, followed by a 10-min waiting time and the second counting interval was 40–60 min. To obtain the activity concentration of ^{212}Pb and ^{212}Bi, the third counting interval was added, following the second counting interval after a 10 min waiting time. Considering the half-lives of ^{212}Pb and ^{212}Bi, the third counting interval could not be too short. Meanwhile, for field measurement, the total measurement cycle

[1] N (6.1 MeV) is α counts in the region 3.0–6.3 MeV, N (7.69 MeV) is α counts in the region 6.5–8.0 MeV, and N (8.78 MeV) is α counts in the region 8.1–10.0 MeV in this paper.

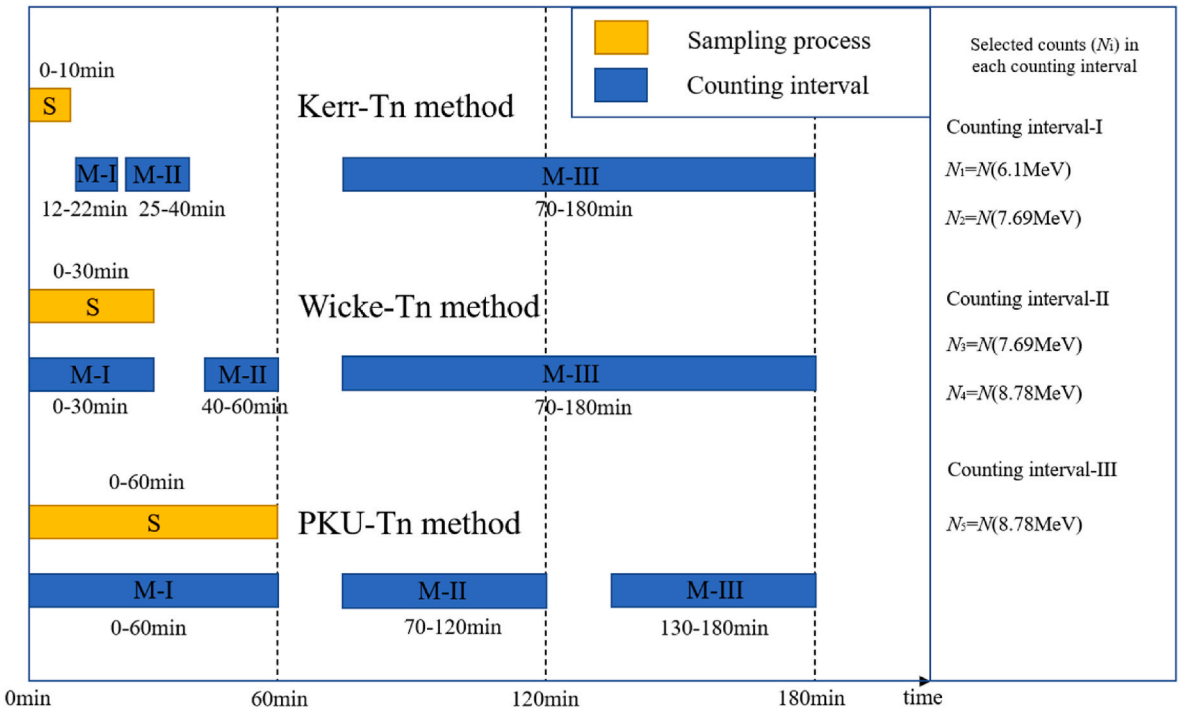

Fig. 1. Sampling and counting intervals of the Kerr-Tn method as reference and the two newly developed methods.

could not be too long. Therefore, the third counting interval of the Wicke-Tn method was selected as 70–180 min and the total measurement cycle was 3 h.

Compared with the Kerr-Tn method, the biggest advantage of the Wicke-Tn method is that the first counting interval is synchronized with sampling time and the lengthened sampling time can greatly increase methodological sensitivity. For further improvement, the synchronizing sampling and counting time was lengthened from 30 to 60 min to enhance the representation of hourly results, and the subsequent counting intervals were adjusted accordingly. Therefore, a new method named the PKU-Tn method was proposed, with the first sampling/counting interval of 0–60 min, a second counting interval of 70–120 min and a third counting interval of 130–180 min.

According to the selected sampling period and three counting intervals, the matrixes can be obtained by substituting time into the formula from the appendix. The corresponding coefficient matrixes of the Wicke-Tn and PKU-Tn methods are shown in Eq. (4) and Eq. (5) separately. The matrix of the Kerr-Tn method with a sightly changed third counting interval from 200-220 to 70–180 min is given in appendix equation (A.8), which limits the total measurement cycle to 3 h.

$$M_{Wicke-Tn\ Method} = \begin{pmatrix} 0.147930 & 0 & 0 & -0.100647 & 0.007200 \\ -0.017814 & -0.051902 & 0.090393 & 0.012120 & -0.000867 \\ 0.001905 & 0.067428 & -0.028386 & -0.001296 & 0.000093 \\ 0 & 0 & 0 & -0.039061 & 0.015745 \\ 0 & 0 & 0 & 0.082804 & -0.007436 \end{pmatrix} \tag{4}$$

$$M_{PKU-Tn\ Method} = \begin{pmatrix} 0.068124 & 0 & 0 & -0.053453 & 0.031287 \\ -0.008521 & -0.009863 & 0.023748 & 0.006686 & -0.003914 \\ 0.001082 & 0.022218 & -0.013178 & -0.000849 & 0.000497 \\ 0 & 0 & 0 & -0.009767 & 0.019422 \\ 0 & 0 & 0 & 0.027378 & -0.019282 \end{pmatrix} \tag{5}$$

2.3. Comparison experiments

To verify the measurement results of the two new methods, a series of comparison experiments were carried out in pure radon, pure thoron and mixed radon–thoron environments, with the Kerr-Tn method taken as the reference method. Comparison experiments were carried out in the radon chamber at the Institution of NBC Defense, which is a stainless-steel chamber with an inner effective volume of nearly 18 m^3, a ^{226}Ra source of nearly 1 MBq was used as radon source and radon concentration was controlled accurately with a computed control system. The temperature and relative humidity could be adjusted and controlled stably in the range of 5–45 °C and 30–95 %, respectively. The radon concentration was recorded automatically by NRM-P01 radon

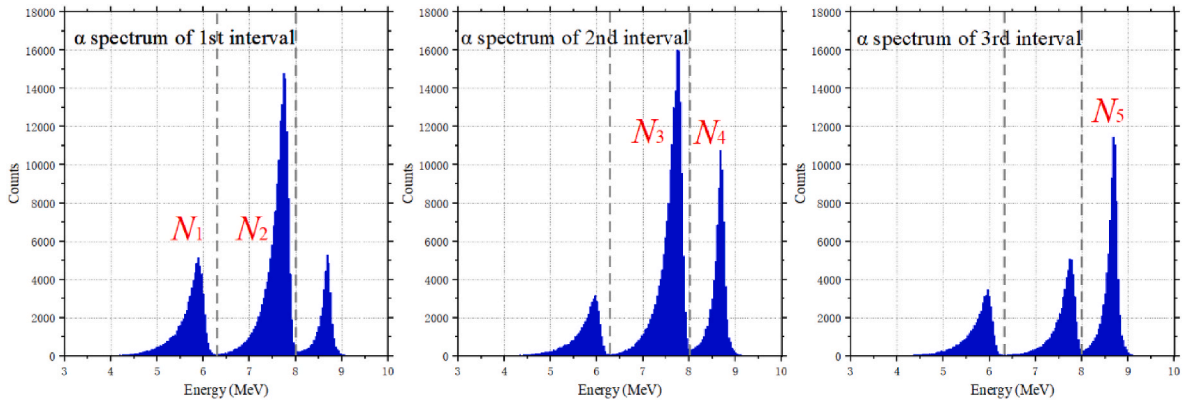

Fig. 2. Typical α spectra of three counting intervals obtained by the PKU-Tn method in a mixed radon–thoron environment.

monitor (Sairatec, n.d.). Aerosol was generated by a condensation monodisperse aerosol generator (Grimm SLG-270, n. d.), and removed by inner air cleaner (NEDFON DGT10-24TP-D, n.d.). A scanning mobility particle sizer (Grimm SMPS-5416, n.d.) was used to monitor the number concentration and the size distribution of the aerosol. The aerosol concentration was controlled around 4×10^4 particles/cm^3, and the median diameter of the particles was nearly 200 nm in the experiments.

To compare the three measurement methods, three step-advanced filter radon progeny monitors RPM-SF01 (Sairatec, n.d.) were employed (Zhang et al., 2017). By pre-setting the measurement procedures, the RPM-SF01 can realize various measurement modes including the aforementioned three measurement methods, and can give ^{218}Po, ^{214}Pb, ^{214}Bi, ^{212}Pb and ^{212}Bi activity concentration with a 3-h cycle. For each RPM-SF01, the flowrate (F) was calibrated to (2.500 ± 0.010) L/min by a Gilian Gilibrator-2 soap bubble flowmeter (Sensidyne, n.d.). The α detection efficiencies (ε_α) of the three instruments were calibrated by ^{241}Am–^{239}Pu electroplating surface source, and the average ε_α values were (21.1 ± 1.0) %. The collection efficiency of the 0.45-μm PTFE filter was nearly 100 %, and so its uncertainty is ignored. The distance between detector and filter was nearly 3 mm, while the α spectrum was broadened with a tail. In the typical α spectra of three counting intervals obtained by the PKU-Tn method in a mixed radon–-thoron environment (Fig. 2), although the α peaks all have tails, α peaks in different ROIs are clearly distinguished, and the crosstalk caused by the tails is likely negligible. Then the uncertainty of radon/thoron progeny concentrations can be calculated using Eq. (3).

Experiment I was carried out in a pure radon environment, with pure radon concentration at about 10^4 Bq/m^3, and aerosol concentration from 10^3 to 4×10^4 cm^{-3}. Experiment I lasted for about 36 h, with the equilibrium equivalent concentration for Rn (EEC_{Rn}) varying in the range of 1600–7000 Bq/m^3.

Experiment II was carried out in a pure thoron environment. To create an environment with only thoron, the residual radon gas in the chamber was purified with activated charcoal before the experiment. After purification, a batch of gas mantles was used as the thoron source (Wang et al., 2017), hanging dispersedly inside the radon chamber and six big inner fans were used to keep progeny distributed uniformity. Experiment II lasted for about 96 h, with EEC_{Tn} varying in the range of nearly 300–500 Bq/m^3.

Experiment III was carried out in a mixed radon–thoron environment. To create a mixed radon–thoron environment, the thoron source was more added in the radon chamber while the radon gas was input into the chamber through the radon source controlling system. Experiment III lasted for more than 50 h, with EEC_{Rn} ranging within 3500–6500 Bq/m^3 and EEC_{Tn} within 1500–3500 Bq/m^3.

3. Results and discussion

3.1. Comparison of three measurement methods in different environments

Comparison of the three measurement methods in pure and mixed radon–thoron environments are shown in Fig. 3. Results of the activity concentrations of EEC_{Rn}, ^{218}Po, ^{214}Pb, ^{214}Bi, EEC_{Tn}, ^{212}Pb and ^{212}Bi of different methods and their average concentrations for the three measurement methods in different environments are summarized in Table 1.

All three measurement methods could respond to the variation of radon/thoron concentrations in pure and mixed radon–thoron environments (Fig. 3), which gave individual radon/thoron progeny concentrations as well as EEC_{Rn}/EEC_{Tn}. Compared with the hourly average value of three methods (Fig. 2), both new methods gave a deviation of EEC_{Rn} from −6.4 % to 5.0 %, and of EEC_{Tn} from −11.8 % to 13.3 %; for each progeny activity concentration, ^{218}Po was within ±18.0 %, ^{214}Pb within ±16.0 %, ^{214}Bi within ±9.7 %, ^{212}Pb within ±11.2 % and ^{212}Bi within ±15.9 %. Considering the variety of progeny concentrations during different sampling processes and measurement uncertainty of different methods, consistency was achieved.

Table 1 gives the average EEC_{Rn}/EEC_{Tn} and radon/thoron progeny activity concentrations of three measurement methods in different environments during the whole period. In the three environments, the standard deviations of activity concentrations for the two new methods were both lower than those for the Kerr-Tn method due to higher counting rate and lower counting uncertainty. The relative deviations of the two new methods compared with the Kerr-Tn method are also shown in Table 1. In a pure radon environment, the relative deviation of Wicke-Tn method was from −7.8 % to 6.2 %, while for the PKU-Tn method, it was 3.4–9.8 %. In a pure thoron environment, the relative deviation of the Wicke-Tn method to the Kerr-Tn method was from −4.6 % to −3.2 %, while for the PKU-Tn method, it was from −7.8 % to −3.8 %. In the mixed radon–thoron environment, the relative deviation of the Wicke-Tn method to the Kerr-Tn method was from −4.4 % to 5.1 %, while for the PKU-Tn method, it was from −6.1 % to 5.5 %. Considering that the relative uncertainty of the detection efficiency $\sigma_{\varepsilon_\alpha}/\ C_{\sigma_{\varepsilon_\alpha}}$ was ±1.0 % and the relative uncertainty of the flow rate $\sigma_F/\ C_{\sigma_F}$ was ±4.0 %, as well as the statistical uncertainty, the relative uncertainty of radon progeny concentrations given by the two new methods were both within ±6.0 %,

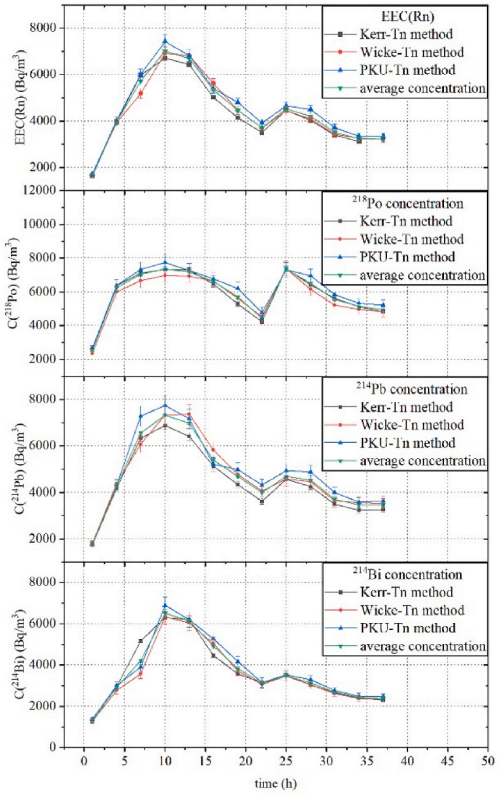

(a)

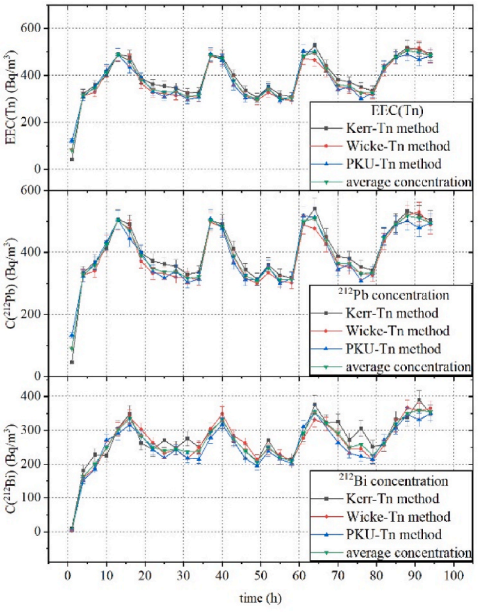

(b)

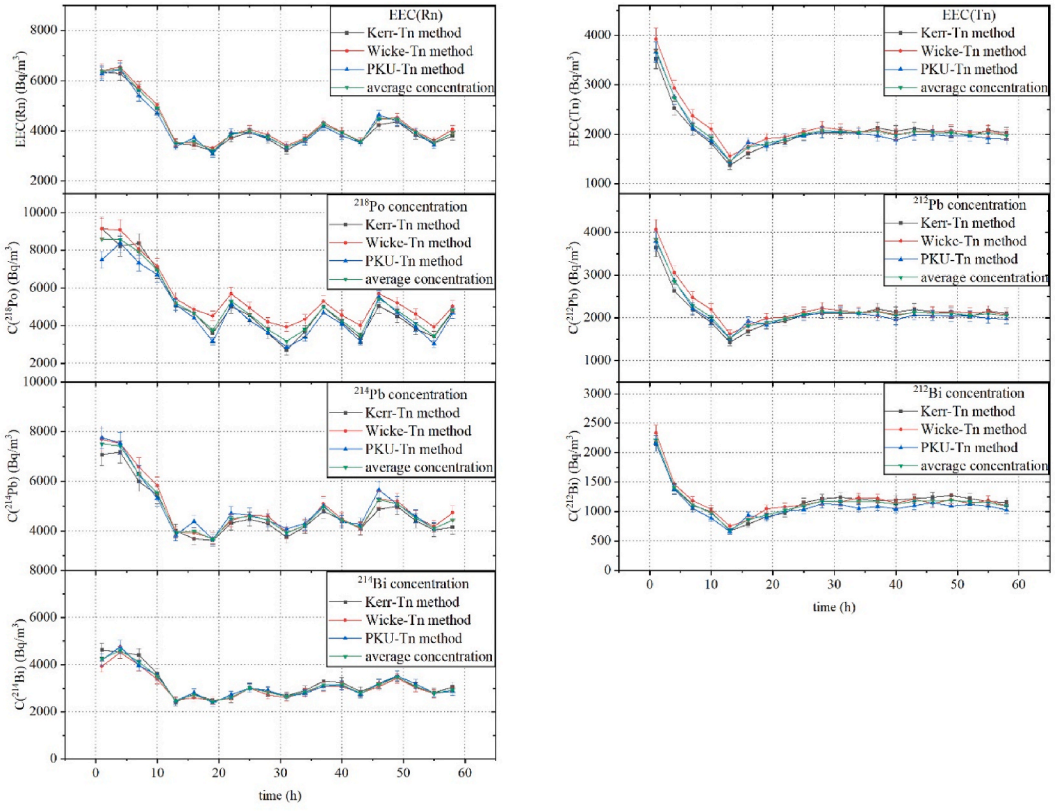

(c)

Fig. 3. Comparison of three measurement methods in (a) pure radon, (b) pure thoron and (c) mixed radon–thoron environments.

Table 1
Average concentrations for the three measurement methods in different environments.

Measurement environments		Activity concentration of different measurement methods (Bq/m^3)				
		Kerr-Tn method	Wicke-Tn method	Relative deviation[a]	PKU-Tn method	Relative deviation
Pure radon	EEC_{Rn}	4346 ± 210	4390 ± 170	1.0 %	4650 ± 180	7.0 %
	$C(^{218}Po)$	6040 ± 590	5570 ± 330	−7.8 %	6260 ± 370	3.6 %
	$C(^{214}Pb)$	4510 ± 440	4790 ± 280	6.2 %	4950 ± 290	9.8 %
	$C(^{214}Bi)$	3655 ± 350	3510 ± 210	−4.0 %	3780 ± 220	3.4 %
Pure thoron	EEC_{Tn}	391 ± 30	375 ± 21	−4.1 %	376 ± 21	−3.8 %
	$C(^{212}Pb)$	413 ± 37	394 ± 23	−4.6 %	395 ± 23	−4.4 %
	$C(^{212}Bi)$	281 ± 25	272 ± 17	−3.2 %	259 ± 16	−7.8 %
Mixed radon–thoron	EEC_{Rn}	4150 ± 240	4280 ± 170	3.1 %	4120 ± 160	−0.7 %
	$C(^{218}Po)$	4980 ± 500	5180 ± 320	4.0 %	4780 ± 280	−4.0 %
	$C(^{214}Pb)$	4690 ± 460	4930 ± 290	5.1 %	4950 ± 290	5.5 %
	$C(^{214}Bi)$	3200 ± 310	3060 ± 180	−4.4 %	3140 ± 180	−1.9 %
	EEC_{Tn}	2060 ± 150	2160 ± 120	4.9 %	2050 ± 120	−0.5 %
	$C(^{212}Pb)$	2140 ± 180	2240 ± 130	4.7 %	2130 ± 130	−0.5 %
	$C(^{212}Bi)$	1175 ± 87	1191 ± 73	1.4 %	1103 ± 68	−6.1 %

[a] Relative deviation with reference method $\sigma_{C_i}/C_{referencee} = (C_i - C_{reference})/C_{reference} \times 100$ %.

Table 2
Average normalized counts for the three measurement methods in different environments.

Measurement environments	EEC	Ratio of progeny concentration	Normalized counts	Measurement methods				
				Kerr-Tn method	Wicke-Tn method	Relative ratio[a]	PKU-Tn method	Relative ratio
Pure radon	EEC_{Rn} (4098 Bq/m^3)	$C(^{218}Po):C(^{214}Pb):C(^{214}Bi)$ = 1:0.70:0.48	N1/ε/F	3919	40,333	10.3	106,792	27.3
			N2/ε/F	32,896	137,567	4.2	602,594	18.3
			N3/ε/F	29,278	151,429	5.2	508,993	17.4
			Total	**66,093**	**329,329**	**5.0**	**1,218,379**	**18.4**
Pure thoron	EEC_{Tn} (421 Bq/m^3)	$C(^{212}Pb):C(^{212}Bi)$ = 1:0.58	N4/ε/F	1776	8578	4.8	40,921	23.0
			N5/ε/F	15,730	47,649	3.0	43,877	2.8
			Total	**19,766**	**64,727**	**3.3**	**113,511**	**5.7**
Mixed radon–thoron	EEC_{Rn} (3842 Bq/m^3)	$C(^{218}Po):C(^{214}Pb):C(^{214}Bi)$ = 1:0.85:0.50	N1/ε/F	7202	54,963	7.6	152,106	21.1
			N2/ε/F	20,255	89,692	4.4	345,515	17.1
			N3/ε/F	28,914	109,510	3.8	358,804	12.4
	EEC_{Tn} (2088 Bq/m^3)	$C(^{212}Pb):C(^{212}Bi)$ = 1:0.52	N4/ε/F	8015	32,934	4.1	173,547	21.7
			N5/ε/F	71,958	198,936	2.8	192,894	2.7
			Total	**136,344**	**486,035**	**3.6**	**1,222,866**	**9.0**

[a] Relative ratio = multiple that the Wicke-Tn/PKU-Tn method compared to the Kerr-Tn method

much lower than for the Kerr-Tn method with ±9.8 %. The thoron progeny concentrations for the two new methods were ±6.0 % and ±7.0 %, which were also lower than ±9.0 % for the Kerr-Tn method. Low measurement uncertainty is better for accurate measurements.

3.2. Uncertainty and sensitivity analysis

To compare the methodological sensitivity of different methods, the normalized counts were defined according to Wang (2021), where the α particles counts were normalized per unit of detection efficiency and per flow rate at a unit or certain EEC_{Rn}/EEC_{Tn}. Then the difference between detection efficiency and flow rate of different measurement systems could be eliminated. The magnitude of the normalized counts characterizes the methodological sensitivity. The higher is the methodological sensitivity, the higher the normalized counts will be. Average normalized counts given by the three different methods in different environments are shown in Table 2.

The methodological sensitivity of the PKU-Tn and Wicke-Tn methods was much higher than that of the Kerr-Tn method and the total counts were 18.4 and 5.0 times higher than that of the Kerr-Tn method in a pure radon environment, respectively, but 5.7 and 3.3 times higher in a pure thoron environment. In a mixed radon–thoron environment, the total counts of the PKU-Tn and Wicke-Tn methods were 9.0 and 3.6 times higher than that of the Kerr-Tn method, respectively.

Although the exact multiples of methodological sensitivity differed in the different environments, the methodological sensitivity of the PKU-Tn method was clearly the highest in all three methods. It is also noteworthy that the N_1 normalized counts ($N_1/\varepsilon/F$) of the PKU-Tn method were more than 20 times higher than that of the Kerr-Tn method, indicating that it was easier to measure ^{218}Po with the PKU-Tn method, despite this being hard to measure in an actual environment due to its short half-life. Significantly, only the PKU-Tn method's sampling time was 1 h among the three methods, which better reflects the hourly variation of radon and thoron progeny concentrations in a real environment. In a typical indoor environment with EEC_{Rn} = 24 Bq/m^3, $C(^{218}Po):C(^{214}Pb):C(^{214}Bi)$ of 1:0.65:0.4, EEC_{Tn} = 0.8 Bq/m^3, and $C(^{212}Pb):C(^{212}Bi)$ nearly 1:1 (UNSCEAR, 2000), the calculated (N_1, N_2, N_3, N_4, N_5) was (15, 66, 98, 3, 18) by Kerr-Tn, (142, 252, 319, 9, 49) by Wicke-Tn and (258, 811, 881, 37, 36) by PKU-Tn method. Furthermore, the first part of Eq. (3), $\left(\frac{M_{i1}{}^2 \bullet N_1 + M_{i2}{}^2 \bullet N_2 + M_{i3}{}^2 \bullet N_3 + M_{i4}{}^2 \bullet N_4 + M_{i5}{}^2 \bullet N_5}{(M_{i1} \bullet N_1 + M_{i2} \bullet N_2 + M_{i3} \bullet N_3 + M_{i4} \bullet N_4 + M_{i5} \bullet N_5)^2}\right)$, i = 1–5, can be calculated as (29 %, 37 %, 42 %, 55 %, 99 %) by Kerr-Tn, (8.8 %, 14 %, 15 %, 40 %, 64 %) by Wicke-Tn and (6.9 %, 7.1 %, 11 %, 40 %, 62

%) by the PKU-Tn method. Thus both the Wicke-Tn and PKU-Tn methods greatly decreased the statistical deviation of counts, leading to a much lower uncertainty and more accurate measurement in the field.

Using the background counting rates of RPM-SF01 system (Zhang et al., 2017), the low level detection limits of different methods could be evaluated using the equation in Wang et al. (2021). For the Kerr-Tn method, the minimum detectable radon and thoron equilibrium activity concentrations were 2.2 and 0.56 Bq/m^3, respectively; for the Wicke-Tn method, these were 0.54 and 0.19 Bq/m^3. For the PKU-Tn method, they were 0.27 and 0.16 Bq/m^3, which were 12 % and 29 % of the value for the Kerr-Tn method, respectively, using the same RPM-SF system.

4. Conclusion

In order to find more sensitive measurement methods of radon and thoron progeny concentration, two new α spectrometry methods were proposed: Wicke-Tn and PKU-Tn methods. Compared with the Kerr-Tn method, two new methods' first counting intervals were synchronized with the sampling process. Furthermore, the PKU-Tn method sampling time was increased to 60 min, in accordance with hourly variation of activity concentration.

Verification results showed that the radon and thoron progeny concentrations obtained by the Wicke-Tn and PKU-Tn methods in three different environments were consistent with those obtained by the Kerr-Tn method. In a mixed radon–thoron environment, the methodological sensitivities of the PKU-Tn and Wicke-Tn methods were 9.0 and 3.6 times higher than that of the Kerr-Tn method, leading to lower uncertainty and higher accuracy. Those improvements are quite important for field measurement at low concentrations. Among the three methods, the PKU-Tn method had the highest methodological sensitivity, lowest detection limit and broader application in future.

It is noteworthy that these two new methods were compared only with the α spectrometry method, with no assumption about radon/thoron progeny ratio, and individual radon/thoron progeny concentrations as well as EEC could be given at the same time. No comparison was made with those spectrometric algorithms which only give single potential α concentration or radon progeny concentration. Further comparison experiments using different methods and devices in different environments will be carried out and the influence of progeny concentration ratio will be discussed in the future.

CRediT authorship contribution statement

Kang Peng: Writing – review & editing, Writing – original draft, Validation, Methodology, Investigation, Formal analysis, Data curation, Conceptualization. **Hao Wang:** Writing – review & editing, Validation, Project administration, Data curation. **Jinmin Yang:** Writing – review & editing, Validation, Data curation. **Lei Zhang:** Writing – review & editing, Supervision, Project administration, Funding acquisition, Formal analysis, Conceptualization. **Qiuju Guo:** Writing – review & editing, Supervision, Resources, Project administration, Funding acquisition, Formal analysis, Conceptualization.

Declaration of competing interest

The authors declare that they have no known competing financial interests or personal relationships that could have appeared to influence the work reported in this paper.

Data availability

Data will be made available on request.

Acknowledgements

This study is financially supported by the National Natural Science Foundation of China (Nos. 12275008 and 12375319).

Appendix

According to the coefficient matrix element formulas given by Wang et al. (2021), the N_1* and N_i (i = 2,3) (which is defined above) can be expressed by radon progeny concentration C_i (i = 1,2,3) as follows. If the first counting interval is synchronized with sampling process (Wicke-Tn and PKU-Tn methods), the relationship can be expressed as Eq. (A.1). If the first counting interval is after the sampling process (Kerr-Tn method), the formulas can be expressed as Eq. (A.2). In order to simplify formulas, take three counting intervals as A, B and C in sequence, where t_{A1} is the beginning moment of the first counting interval and t_{A2} is the end moment of the first counting interval.

$$
\begin{cases}
N_1^* = \varepsilon_a F \varepsilon_F \bullet g(\lambda_1, t_{A1}, t_{A2}) \bullet C_1 \\
N_2 = \varepsilon_a F \varepsilon_F \left[\lambda_2\lambda_3 \left[\dfrac{g(\lambda_1, t_{A1}, t_{A2}) - g(\lambda_2, t_{A1}, t_{A2})}{(\lambda_3 - \lambda_1)(\lambda_2 - \lambda_1)} - \dfrac{g(\lambda_2, t_{A1}, t_{A2}) - g(\lambda_3, t_{A1}, t_{A2})}{(\lambda_3 - \lambda_1)(\lambda_3 - \lambda_2)} \right] C_1 \right. \\
\qquad \left. + \lambda_3 \bullet \dfrac{g(\lambda_2, t_{A1}, t_{A2}) - g(\lambda_3, t_{A1}, t_{A2})}{\lambda_3 - \lambda_2} \bullet C_2 + g(\lambda_3, t_{A1}, t_{A2}) \bullet C_3 \right] \\
N_3 = \varepsilon_a F \varepsilon_F \left[\lambda_2\lambda_3 \left(\dfrac{1 - e^{-\lambda_1 t_{se}}}{\lambda_1} \bullet \left[\dfrac{h(\lambda_1, t_{B1}, t_{B2}) - h(\lambda_2, t_{B1}, t_{B2})}{(\lambda_3 - \lambda_1)(\lambda_2 - \lambda_1)} - \dfrac{h(\lambda_2, t_{B1}, t_{B2}) - h(\lambda_3, t_{B1}, t_{B2})}{(\lambda_3 - \lambda_1)(\lambda_3 - \lambda_2)} \right] \right. \right. \\
\qquad + \dfrac{1}{\lambda_2 - \lambda_1} \left(\dfrac{1 - e^{-\lambda_1 t_{se}}}{\lambda_1} - \dfrac{1 - e^{-\lambda_2 t_{se}}}{\lambda_2} \right) \bullet \dfrac{h(\lambda_2, t_{B1}, t_{B2}) - h(\lambda_3, t_{B1}, t_{B2})}{\lambda_3 - \lambda_2} \\
\qquad \left. \left. + \left[\dfrac{\dfrac{1 - e^{-\lambda_1 t_{se}}}{\lambda_1} - \dfrac{1 - e^{-\lambda_2 t_{se}}}{\lambda_2}}{(\lambda_3 - \lambda_1)(\lambda_2 - \lambda_1)} - \dfrac{\dfrac{1 - e^{-\lambda_2 t_{se}}}{\lambda_2} - \dfrac{1 - e^{-\lambda_3 t_{se}}}{\lambda_3}}{(\lambda_3 - \lambda_1)(\lambda_3 - \lambda_2)} \right] \bullet h(\lambda_3, t_{B1}, t_{B2}) \right) C_1 \right. \\
\qquad + \lambda_3 \left(\dfrac{1 - e^{-\lambda_2 t_{se}}}{\lambda_2} \bullet \dfrac{h(\lambda_2, t_{B1}, t_{B2}) - h(\lambda_3, t_{B1}, t_{B2})}{\lambda_3 - \lambda_2} \right. \\
\qquad \left. + \dfrac{\dfrac{1 - e^{-\lambda_2 t_{se}}}{\lambda_2} - \dfrac{1 - e^{-\lambda_3 t_{se}}}{\lambda_3}}{\lambda_3 - \lambda_2} \bullet h(\lambda_3, t_{B1}, t_{B2}) \right) C_2 \\
\qquad \left. + \dfrac{1 - e^{-\lambda_3 t_{se}}}{\lambda_3} \bullet h(\lambda_3, t_{B1}, t_{B2}) \bullet C_3 \right]
\end{cases}
\tag{A.1}
$$

$$
\begin{cases}
N_1^* = \varepsilon_\alpha F \varepsilon_F \bullet \dfrac{1-e^{-\lambda_1 t_{se}}}{\lambda_1} h(\lambda_1, t_{A1}, t_{A2}) \bullet C_1 \\
N_2 = \varepsilon_\alpha F \varepsilon_F \left[\lambda_2\lambda_3 \left(\begin{array}{l} \dfrac{1-e^{-\lambda_1 t_{se}}}{\lambda_1} \bullet \left[\dfrac{h(\lambda_1, t_{A1}, t_{A2}) - h(\lambda_2, t_{A1}, t_{A2})}{(\lambda_3-\lambda_1)(\lambda_2-\lambda_1)} - \dfrac{h(\lambda_2, t_{A1}, t_{A2}) - h(\lambda_3, t_{A1}, t_{A2})}{(\lambda_3-\lambda_1)(\lambda_3-\lambda_2)} \right] \\ + \dfrac{1}{\lambda_2-\lambda_1} \left(\dfrac{1-e^{-\lambda_1 t_{se}}}{\lambda_1} - \dfrac{1-e^{-\lambda_2 t_{se}}}{\lambda_2} \right) \bullet \dfrac{h(\lambda_2, t_{A1}, t_{A2}) - h(\lambda_3, t_{A1}, t_{A2})}{\lambda_3-\lambda_2} \\ + \left[\dfrac{\dfrac{1-e^{-\lambda_1 t_{se}}}{\lambda_1} - \dfrac{1-e^{-\lambda_2 t_{se}}}{\lambda_2}}{(\lambda_3-\lambda_1)(\lambda_2-\lambda_1)} - \dfrac{\dfrac{1-e^{-\lambda_2 t_{se}}}{\lambda_2} - \dfrac{1-e^{-\lambda_3 t_{se}}}{\lambda_3}}{(\lambda_3-\lambda_1)(\lambda_3-\lambda_2)} \right] \bullet h(\lambda_3, t_{A1}, t_{A2}) \end{array} \right) C_1 \right. \\
\qquad + \lambda_3 \left(\begin{array}{l} \dfrac{1-e^{-\lambda_2 t_{se}}}{\lambda_2} \bullet \dfrac{h(\lambda_2, t_{A1}, t_{A2}) - h(\lambda_3, t_{A1}, t_{A2})}{\lambda_3-\lambda_2} \\ + \dfrac{\dfrac{1-e^{-\lambda_2 t_{se}}}{\lambda_2} - \dfrac{1-e^{-\lambda_3 t_{se}}}{\lambda_3}}{\lambda_3-\lambda_2} \bullet h(\lambda_3, t_{A1}, t_{A2}) \end{array} \right) C_2 \\
\qquad \left. + \dfrac{1-e^{-\lambda_3 t_{se}}}{\lambda_3} \bullet h(\lambda_3, t_{A1}, t_{A2}) \bullet C_3 \right] \\
N_3 = \varepsilon_\alpha F \varepsilon_F \left[\lambda_2\lambda_3 \left(\begin{array}{l} \dfrac{1-e^{-\lambda_1 t_{se}}}{\lambda_1} \bullet \left[\dfrac{h(\lambda_1, t_{B1}, t_{B2}) - h(\lambda_2, t_{B1}, t_{B2})}{(\lambda_3-\lambda_1)(\lambda_2-\lambda_1)} - \dfrac{h(\lambda_2, t_{B1}, t_{B2}) - h(\lambda_3, t_{B1}, t_{B2})}{(\lambda_3-\lambda_1)(\lambda_3-\lambda_2)} \right] \\ + \dfrac{1}{\lambda_2-\lambda_1} \left(\dfrac{1-e^{-\lambda_1 t_{se}}}{\lambda_1} - \dfrac{1-e^{-\lambda_2 t_{se}}}{\lambda_2} \right) \bullet \dfrac{h(\lambda_2, t_{B1}, t_{B2}) - h(\lambda_3, t_{B1}, t_{B2})}{\lambda_3-\lambda_2} \\ + \left[\dfrac{\dfrac{1-e^{-\lambda_1 t_{se}}}{\lambda_1} - \dfrac{1-e^{-\lambda_2 t_{se}}}{\lambda_2}}{(\lambda_3-\lambda_1)(\lambda_2-\lambda_1)} - \dfrac{\dfrac{1-e^{-\lambda_2 t_{se}}}{\lambda_2} - \dfrac{1-e^{-\lambda_3 t_{se}}}{\lambda_3}}{(\lambda_3-\lambda_1)(\lambda_3-\lambda_2)} \right] \bullet h(\lambda_3, t_{B1}, t_{B2}) \end{array} \right) C_1 \right. \\
\qquad + \lambda_3 \left(\begin{array}{l} \dfrac{1-e^{-\lambda_2 t_{se}}}{\lambda_2} \bullet \dfrac{h(\lambda_2, t_{B1}, t_{B2}) - h(\lambda_3, t_{B1}, t_{B2})}{\lambda_3-\lambda_2} \\ + \dfrac{\dfrac{1-e^{-\lambda_2 t_{se}}}{\lambda_2} - \dfrac{1-e^{-\lambda_3 t_{se}}}{\lambda_3}}{\lambda_3-\lambda_2} \bullet h(\lambda_3, t_{B1}, t_{B2}) \end{array} \right) C_2 \\
\qquad \left. + \dfrac{1-e^{-\lambda_3 t_{se}}}{\lambda_3} \bullet h(\lambda_3, t_{B1}, t_{B2}) \bullet C_3 \right]
\end{cases}
\tag{A.2}
$$

Here, N_1* is the net counts from ^{218}Po ($=N_1-0.56N_3$), which is different from the definition above. The expressions of $g(\lambda_i, t_1, t_2)$ and $h(\lambda_i, t_1, t_2)$ are shown as Eq. (A.3); λ_1, λ_2 and λ_3 are the decay constants of ^{218}Po, ^{214}Pb and ^{214}Bi, respectively.

$$
\begin{cases}
g(\lambda_i, t_1, t_2) = \dfrac{t_2-t_1}{\lambda_i} + \dfrac{1}{\lambda_i^2}\left(e^{-\lambda_i t_2} - e^{-\lambda_i t_1}\right) \\
h(\lambda_i, t_1, t_2) = \dfrac{1}{\lambda_i}\left(e^{-\lambda_i t_1} - e^{-\lambda_i t_2}\right)
\end{cases}
\tag{A.3}
$$

Since the decay chain of thoron is similar to that of radon, the expressions for N_4 and N_5 can be written analogically as Eq. (A.4).

$$\begin{cases} N_4 = 0.64 \bullet \varepsilon_\alpha F \varepsilon_F \bullet \left[\lambda_5 \left(\dfrac{1-e^{-\lambda_4 t_{se}}}{\lambda_4} \bullet \dfrac{h(\lambda_4, t_{B1}, t_{B2}) - h(\lambda_5, t_{B1}, t_{B2})}{\lambda_5 - \lambda_4} + \dfrac{\dfrac{1-e^{-\lambda_4 t_{se}}}{\lambda_4} - \dfrac{1-e^{-\lambda_5 t_{se}}}{\lambda_5}}{\lambda_5 - \lambda_4} \bullet h(\lambda_5, t_{B1}, t_{B2}) \right) C_4 + \dfrac{1-e^{-\lambda_5 t_{se}}}{\lambda_5} \bullet h(\lambda_5, t_{B1}, t_{B2}) \bullet C_5 \right] \\ N_5 = 0.64 \bullet \varepsilon_\alpha F \varepsilon_F \bullet \left[\lambda_5 \left(\dfrac{1-e^{-\lambda_4 t_{se}}}{\lambda_4} \bullet \dfrac{h(\lambda_4, t_{C1}, t_{C2}) - h(\lambda_5, t_{C1}, t_{C2})}{\lambda_5 - \lambda_4} + \dfrac{\dfrac{1-e^{-\lambda_4 t_{se}}}{\lambda_4} - \dfrac{1-e^{-\lambda_5 t_{se}}}{\lambda_5}}{\lambda_5 - \lambda_4} \bullet h(\lambda_5, t_{C1}, t_{C2}) \right) C_4 + \dfrac{1-e^{-\lambda_5 t_{se}}}{\lambda_5} \bullet h(\lambda_5, t_{C1}, t_{C2}) \bullet C_5 \right] \end{cases} \quad [A.4]$$

where and λ_4 and λ_5 are the decay constants of ^{212}Pb and ^{212}Bi, respectively.

Since ^{212}Bi has two decay branches, one decay chain produces 8.78 MeV α particles, with a branch ratio of 64 %. The other decay chain produces α particles of 6.1 MeV with a branch ratio of 36 %. The counts of ROI-I obtained during the first counting interval include the α particle interference generated by ^{212}Bi. $N1$ is the counts in the region of 6.0 MeV including those similar α particles from ^{212}Bi.

Therefore, N_i can be totally described by radon and thoron progeny concentration. The linear relationship can be written in the matrix form as Eq. (1) shows, with its elements given by formulas above.

Kerr-Tn method is used as a reference method, while its coefficient matrix formula is given in Kerr (1978). In the initial measurement method given by Kerr, the last counting period was set as 400–420 min. In order to match the new methods' period, the final counting time of the Kerr-Tn method was advanced so that the whole measurement cycle was 3 h. By changing different final counting times, different coefficient matrix elements can be found for which the relative uncertainty of thoron progeny can be minimized when the final counting time is set to 70–180 min. The corresponding coefficient matrix is shown in Eq. (A.8).

$$M_{Kerr-Tn\ Method} = \begin{pmatrix} 1.68559 & 0 & 0 & -0.831410 & 0.028418 \\ -0.207797 & -0.393905 & 0.450152 & 0.102495 & -0.003503 \\ 0.030033 & 0.419736 & -0.192125 & -0.014814 & 0.000506 \\ 0 & 0 & 0 & -0.111719 & 0.041233 \\ 0 & 0 & 0 & 0.277929 & -0.014927 \end{pmatrix} \quad [A.8]$$

References

Bigu, J., Grenier, M., 1984. Thoron daughter working level measurements by one and two gross alpha-count methods. Nucl. Instrum. Methods Phys. Res. 225, 385–398. https://doi.org/10.1016/0167-5087(84)90277-1.

Chalupnik, S., Skubacz, K., Urban, P., Wysocka, M., 2017. Measurements of airborne concentrations of radon and thoron decay products. Radiat. Protect. Dosim. 177, 45–48. https://doi.org/10.1093/rpd/ncx164.

Coté, P., Townsend, M.G., 1981. Mixtures of radon and thoron daughters in underground atmospheres. Health Phys. 40, 5–17. https://doi.org/10.1097/00004032-198101000-00002.

GRIMM Aerosol Technik GmbH & Co. KG. SMPS-5416 scanning mobility particle sizer. www.grimm-aerosol.com.

GRIMM Aerosol Technik GmbH & Co. KG. SLG-270 condensation monodisperse aerosol generator. www.grimm-aerosol.com.

Jenkins, P.H., 2002. Equations for modeling of grab samples of radon decay products. Health Phys. 83, S48–S51. https://doi.org/10.1097/00004032-200208001-00014.

Katona, T., Kanyar, B., Somlai, J., Molnar, A., 2007. Determining ^{222}Rn daughter activities by simultaneous alpha- and beta-counting and modeling. J. Radioanal. Nucl. Chem. 272, 69–74. https://doi.org/10.1007/s10967-006-6793-4.

Kerr, G.D., 1975. Measurement of Radon Progeny Concentrations in Air by Alpha-Particle Spectrometry. No. ORNL-TM–4924. Oak Ridge National Lab. https://inis.iaea.org/collection/NCLCollectionStore/_Public/06/214/6214708.pdf.

Kerr, G.D., Ryan, M.T., Perdue, P.T., 1978. Measurement of Airborne Concentrations of Radon-220 Daughter Products by Alpha-Particle Spectrometry. Oak Ridge National Lab., Tenn. USA. https://www.osti.gov/servlets/purl/5168863.

Khan, A., Busigin, A., Phillips, C.R., 1982. An optimized scheme for measurement of the concentrations of the decay products of radon and thoron. Health Phys. 42, 809–826. https://doi.org/10.1097/00004032-198206000-00006.

NEDFON, Air cleaner DGT10-24TP-D. www.nedfon.com/Product/389.html.

Pressyanov, D.S., Guelev, M.G., Pentchev, O.J., 1993. Integrated measurements of short-lived ^{222}Rn progeny by rotating filter. Health Phys. 64, 522–527. https://doi.org/10.1097/00004032-199305000-00009.

Sairatec Co. Ltd, 2021. RPM-SF01 Radon Progeny Monitor. http://www.sairatec.com/teamvie-w_5999939.html.

Sensidyne, L.P.. Gilian Gilibrator-2 NIOSH primary standard air flow calibrator. https://www.sensidyne.com/air-sampling-equipment/calibration-equipment/gilibrator-2/.

Stajic, J.M., Nikezic, D., 2015. The accuracy of radon and thoron progeny concentrations measured through air filtration. J. Environ. Radioact. 140, 50–58. https://doi.org/10.1016/j.jenvrad.2014.11.002.

Thiessen, N.P., 1994. Alpha particle spectroscopy in radon/thoron progeny measurements. Health Phys. 67, 632–640. https://doi.org/10.1097/00004032-199412000-00006.

Thomas, J.W., 1972. Measurement of radon progeny in air. Health Phys. 23, 783. https://doi.org/10.1097/00004032-197212000-00004.

United Nations Scientific Committee on the Effects of Atomic Radiation (UNSCEAR), 2000. Sources and Effects of Ionizing Radiation, vol. I. United Nations Publications. https://www.unscear.org/unscear/en/publications/2000_1.html.

United Nations Scientific Committee on the Effects of Atomic Radiation (UNSCEAR), 2008. Sources and Effects of Ionizing Radiation, vol. I. United Nations Publications. https://www.unscear.org/unscear/en/publications/2008_1.html.

United Nations Scientific Committee on the Effects of Atomic Radiation (UNSCEAR), 2019. Sources, Effects and Risks of Ionizing Radiation, vol. I. United Nations Publications. https://www.unscear.org/unscear/publications/2019.html.

Wang, Y., Zhang, L., Guo, Q., 2017. The experimental study on the emanation power of a flow-through thoron source made from incandescent gas mantles. J. Radiol. Prot. 18, 918–926. https://doi.org/10.1088/1361-6498/aa869a.

Wang, Y., Sun, C., Zhang, L., Guo, Q., 2021. Optimized method for individual radon progeny measurement based on alpha spectrometry following the Wicke method. Radiat. Meas. 142, 106558 https://doi.org/10.1016/j.radmeas.2021.106558.

Zhang, C., Luo, D., 1983. Measurement of mixed radon and thoron daughter concentrations in air. Nucl. Instrum. Methods 215, 481–488. https://doi.org/10.1016/0167-5087(83)90482-9.

Zhang, L., Yang, J., Guo, Q., 2017. Study on a step-advanced filter monitor for continuous radon progeny measurement. Radiat. Protect. Dosim. 173, 259–262. https://doi.org/10.1093/rpd/ncw333.